JOURNAL OF GEOPHYSICAL RESEARCH, VOL. 99, NO. C6, PAGES 12,471–12,485, JUNE 15, 1994

Thermohaline circulation: Energetics and variability in a single-hemisphere basin model

Rui Xin Huang

Department of Physical Oceanography, Woods Hole Oceanographic Institution, Woods Hole, Massachusetts

Abstract. A series of numerical experiments have been carried out to explore the variability of the thermohaline circulation and the energetics of halocline catastrophe. It is found that when the amplitude of surface freshwater flux is smaller than a critical value, the thermohaline circulation is in a thermal mode, with deep water formed in the north. When the freshwater flux amplitude is supercritical, the thermohaline circulation does not reach a single steady state. Instead, the model ocean is in a continuous transition between a slow, quasi-steady saline mode and an energetic, unsteady thermal mode. For cases with no wind stress, the saline mode is characterized by sinking along the equator. For cases with wind stress, the saline mode is characterized by intermediate water formation at midlatitude. During the saline mode phase, the deep water gradually becomes warm and salty. Thus at the end of the saline mode phase, within the northern basin there is cold and relatively fresh water lying on top of warm and salty water. Such a vertical structure is potentially very unstable because small perturbations can grow, supported by the release of potential energy during strong cooling. A quantity called the diabatic available potential energy index is introduced as an indicator for such convective instability. Thus a final equilibrium in the saline mode cannot be reached; instead, the model ocean flips to a very energetic thermal mode in which violent overturning destroys the vertical stratification. After the energy is released, the saline cell supported by precipitation in the subpolar basin advances southward and the model ocean returns to the saline mode. The whole cycle will be repeated.

1. Introduction

It is well known that the thermohaline circulation in the North Atlantic is very different from that in the North Pacific. The thermohaline circulation in the North Atlantic is characterized by deepwater formation, which induces a conveyor belt transporting warm and salty surface water poleward. The conveyor belt gives rise to high surface salinity and a large poleward heat flux, pushing the ice margin to about 70°N.

The thermohaline circulation in the North Pacific is characterized by intermediate water formation. Since no deep water is formed, there is no conveyor belt in the North Pacific. Accordingly, the subpolar gyre of the North Pacific is relatively cold, which gives rise to low evaporation and low salinity, and the ice margin is located around 60°N.

There have been many theories about the mechanisms responsible for the remarkable differences between these two oceans. *F. Bryan* [1986] successfully found multiple equilibria of the thermohaline circulation in a primitive numerical model. His work shed light on the link between the highly idealized two-box model of *Stommel* [1961] and the real oceans. It became clear that the thermohaline circulation in the North Atlantic is thermal dominated (a thermal mode), while the thermohaline circulation in the North Pacific is saline dominated (a saline mode). The thermal mode is characterized by cold water sinking at high latitudes and a strong meridional overturning. The saline mode is characterized by a halocline at high latitudes which prevents deep water formation there, and the meridional overturning is rather weak.

During the past few years, thermohaline circulation variability on timescales from decadal to millennial has been studied by many investigators. The collapse of the saline-dominated circulation and its return to the thermally dominated circulation, the so-called flushing, has been described by *Marotzke* [1989]. *Weaver and Sarachik* [1991] studied the variability of thermohaline circulation and its sensitivity to the so-called mixed boundary conditions. As shown by Weaver and Sarachik, the model's behavior is very sensitive to small changes in the salt flux profile. There have been many other studies devoted to these topics [e.g., *Weaver et al.*, 1991; *Wright and Stocker*, 1991; *Weaver et al.*, 1993; *Winton and Sarachik*, 1993.]

Most of these experiments have been based on the Geophysical Fluid Dynamics Laboratory (GFDL) model formulated upon the virtual salt flux. Usually, a model

Paper number 94JC00522.
0148-0227/94/94JC-00522$05.00

ocean is spun-up under the relaxation condition for both temperature and salinity. After the model ocean reaches a quasi-steady state, the equivalent salt flux required for maintaining the salinity balance is diagnosed. The model ocean is then restarted from such a quasi-steady state and run under a combination of a relaxation condition for temperature and a salt flux condition for salinity, the so-called mixed boundary conditions.

However, there are subtle differences between thermal and saline forcing. In fact, thermal forcing is a heat flux, a thermal energy flux, while saline forcing is a freshwater flux, a mass flux, not really an energy flux (although there is some potential energy associated with the fresh water entering the upper surface and some energy associated with the chemical potential, but such energy seems relatively small). Thermal forcing is associated with very strong negative feedback between the heat flux and the local surface temperature, while there is no feedback between the freshwater flux and the local salinity. Accordingly, the suitable upper boundary condition for thermal forcing can be written as

$$k\frac{\partial T}{\partial z} = \Gamma(T^* - T_s) \qquad z = \eta \ ,$$

where k is the vertical diffusivity, Γ is the relaxation constant, T^* is the so-called reference temperature, although in many models the climatological mean surface temperature is used as the T^*, T_s is the surface temperature, and η is the free surface [*Haney*, 1971].

The suitable upper boundary conditions for the salt balance are

$$w^* = E - P, \quad F_s = wS - k\frac{\partial S}{\partial z} = 0 \qquad z = \eta \ ,$$

where w^* is the Lagrangian vertical velocity across the air–sea interface, $E - P$ is evaporation minus precipitation; the second boundary condition guarantees that F_s (the salt flux across the air–sea interface) is zero, w is the vertical velocity, S is the salinity.

Although such natural boundary conditions for the salinity balance have been known for years, they have seldom been used in oceanic models for some technical reasons. First, there are great uncertainties in the global evaporation and precipitation measurements. Second, models based on flux conditions tend to drift away from the present-day climate. Instead, the same relaxation condition used for temperature has also been used for salinity, even with the same relaxation coefficient. The problems associated with using the relaxation condition for salinity have been realized, and the so-called mixed boundary conditions have been used instead for some numerical models, in which the salinity is forced by a virtual salt flux

$$k\frac{\partial S}{\partial z} = (E - P)\overline{S}_s$$

where $\overline{S}_s$ is the mean surface salinity of the model ocean. The limitations of both these boundary conditions have been discussed by *Huang* [1993], and a natural and more accurate upper boundary condition (the freshwater flux) has also been proposed and tested.

The other subtle difference between thermal and freshwater forcing is in their "relaxation time." For a simple thermally forced model, the temperature change can be described by

$$\frac{dT}{dt} = \frac{\Gamma}{H}(T^* - T)$$

where $\Gamma = 0.7$ m d^{-1} and $H = 30$ m (for the upper layer of the model). Therefore, the e-folding time for temperature is

$$\tau_t = \frac{H}{\Gamma} \approx 43 \text{ d}$$

For a freshwater-forced layer, the salinity changes according to

$$[H + (P - E)t]\,S = HS_0 \ ,$$

where the amplitude of $E - P$ is about 1 m yr^{-1}; so the e-folding time for precipitation is

$$\tau_s = \frac{H}{P}(e - 1) \approx 51 \text{ yr} \ ,$$

and the equivalent time for evaporation is

$$\tau_s = \frac{H}{E}\left(1 - \frac{1}{e}\right) \approx 19 \text{ yr}$$

Accordingly, the salinity anomaly can live at least a hundred times longer than the temperature anomaly. The difference in the relaxation times has a profound impact on the temporal evolution and final structure of the thermohaline circulation, and this is a major issue to be explored in this study. Because the relaxation time for the temperature is substantially shorter than that of salinity, a situation where cold and fresh water overlies warm and salty water can be unstable to convective overturning. This is explained in the appendix, where an energy index for supporting such an instability, the diabatic available potential energy index (DAPEI) is introduced.

In some of the earlier studies, the meridional salt flux diagnosed from models based on a virtual salt flux condition was used for interpolating the flushing [e.g., *Winton and Sarachik*, 1993]. However, the meridional salt flux calculated from these models neglects a major term due to the meridional barotropic flow because the vertically integrated horizontal velocity in these models has no divergence. In a model based on natural boundary conditions for salinity, freshwater flux and salt flux through the oceans are simulated accurately. As shown by *Huang* [1993], the meridional salt flux calculated from the new model is 10 times smaller than that from the old models, and sometimes even the sign is different. Therefore it is clear that caution must be taken in interpolating the physical meaning of the meridional salt flux calculated from these old models. A major point of our study is to show that flushing observed in

many numerical experiments is indeed supported from the energy released during the strong cooling. Such energy release requires a precondition associated with the vertical temperature/salinity gradient, so the DAPEI can be used as a useful indicator.

The difference in the upper boundary conditions also gives rise to quite different basic scales for the circulations forced by heat flux or freshwater flux. This issue has been discussed by *Huang and Chou* [1994]. The oscillatory nature of the model depends on the upper boundary conditions. Thus even small changes in the upper boundary conditions may give rise to different oscillatory behavior. For example, under the same precipitation minus evaporation forcing, the model based on the natural boundary conditions for the salinity balance has a simple limit cycle of an 18.87-year period, while the model based on the old boundary conditions has a limit cycle of 40.38 yrs (period doubling) [*Huang*, 1993]. Thus another goal of this study is to examine the variability of the new model.

In this study, the focus will be on the different patterns of thermohaline circulation controlled by the amplitude of freshwater flux. A concise description of the numerical model is presented in section 2. The thermohaline circulation is a strongly nonlinear phenomenon, so the resulting circulation is not a simple linear superposition of the thermal circulation and the saline circulation. This nonlinear nature of the thermohaline circulation is discussed briefly in section 3. The first set of numerical experiments is designed for the purely thermohaline circulation (without wind stress forcing); the structure of the thermohaline circulation and flushing phenomenon is discussed in section 4. The combined wind-driven circulation and thermohaline circulation is presented in section 5, with emphasis on thermohaline catastrophe, flushing, and its energetics. The main results from this study are summarized and discussed in section 6.

2. Numerical Model

The numerical model used in this study is the Geophysical Fluid Dynamics Laboratory (GFDL) primitive equation model [*Bryan*, 1969; *Cox*, 1984], with some modifications to the upper boundary conditions for salinity. Under the rigid lid approximation, the new upper boundary conditions for the salinity balance are

$$w_0 = E - P\,, \qquad z = 0\,;$$

and a no-salt flux condition

$$F_s = wS - kS_z = 0\,, \qquad z = 0\,.$$

This boundary condition is valid for climate mean circulation of timescales longer than interannual [*Huang*, 1993].

In some earlier studies [e.g., *Weaver et al.*, 1991, 1993], chaotic oscillations and flushing seem to depend on special profiles of evaporation minus precipitation. In this study a simple, "linear" profile is chosen for a basin confined between the equator $\phi = 0$ and the northern boundary $\phi = \phi_n$, as

$$w_0 = \frac{W_0}{\cos\phi}\left(1 - \frac{2\phi}{\phi_n}\right)\,,$$

where $W_0 > 0$ characterizes the amplitude of freshwater flux. This simple profile has been chosen to demonstrate that the oscillatory nature of the thermohaline circulation is intrinsic to the large amplitude of fresh-

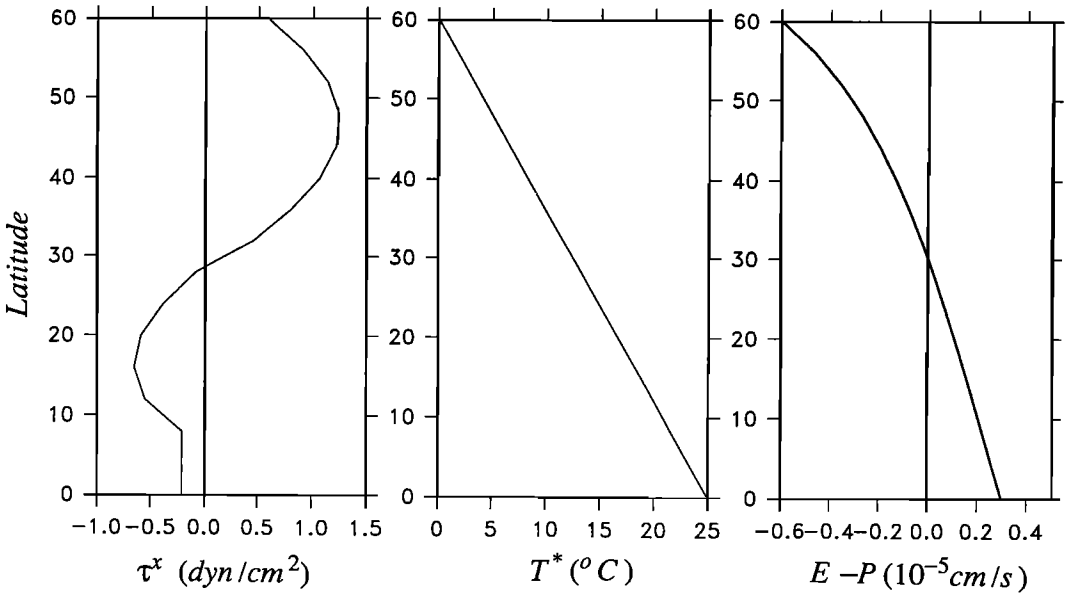

Figure 1. Forcing fields for the model ocean, zonal wind stress τ^x, reference temperature T^*, and evaporation minus precipitation $E - P$, $w_0 = 1$ m yr^{-1}.

water flux. In fact, numerical experiments show that under the simple "linear profile," the thermohaline circulation starts to oscillate or flush as long as the amplitude of freshwater flux is higher than some critical value; more realistic freshwater profiles only add some complexity to the oscillation.

The upper boundary condition for the temperature is a relaxation condition

$$k\frac{\partial T}{\partial z} = \Gamma(T^* - T) ,$$

with a relaxation constant of 0.70 m d^{-1}, which is equivalent to a relaxation time of 43 days for an upper layer 30 m thick.

The model is a 60° × 60° basin, mimicking the North Atlantic, with a horizontal resolution of 4° × 4° and 15 levels vertically. The horizontal viscosity coefficient is 10^9 cm^2 s^{-1}, the horizontal diffusivity coefficient is 10^7 cm^2 s^{-1}, and the vertical viscosity and diffusivity coefficients are 1 cm^2 s^{-1}; these coefficients are typical for such lower resolution models. The time step for the momentum equation is 7200 s and 172,000 seconds for the tracers. For all the numerical experiments discussed in this study the model ocean is spun-up from an initially homogeneous ocean with a temperature of 12.5°C and salinity 35 practical salinity units (psu).

The model's forcings are summarized in Figure 1, including the wind stress, the reference temperature, and the freshwater flux. The same boundary conditions are used throughout each numerical experiment. The amplitude of the thermal forcing will be fixed in this study, while the amplitude of the freshwater flux will be varied in order to explore the thermohaline circulation change in response to different amounts of effective evaporation minus precipitation.

In the following discussion, the notations for the experiments are as follows: F indicates a model forced by freshwater flux alone; TF indicates a model forced by thermal forcing and freshwater flux, and WTF indicates a model forced by wind stress, thermal and freshwater forcings.

3. Nonlinear Nature of the Coupled Wind-Driven and Thermohaline Circulation

The general circulation in the oceans is the result of the competition between three forcings, i.e., the wind stress, the heat flux, and the freshwater flux. The outcome of these forcings is far from being a simple linear superposition. Table 1 lists the results from four experiments. The first one, case F, is a saline circulation forced by freshwater flux alone (the amplitude is 0.5 m yr^{-1}), with a meridional circulation of −85.8 Sv (negative sign indicates sinking at the equator); while the second one, case T, is a thermal circulation forced by a thermal relaxation condition, with a meridional circulation of 25.70 Sv (sinking in the north).

Although the thermal forcing alone seems much less efficient than the freshwater forcing in terms of driving the meridional circulation, the result of combining these two forcings is a circulation in the thermal mode. In general, the circulation in case TF is rather similar to that of case T with minor differences. For example, now the meridional circulation is slightly weak, a decline from 25.70 Sv for the purely thermal-forced case to 22.70 Sv for the combined thermohaline case. Accordingly, the basinwide temperature is slightly warmer, and the mean kinetic energy is lower.

When the wind stress is included (case WTF-1), the meridional overturning does not change much. Apparently, the meridional circulation in this case is primarily determined by the thermohaline forcings and the wind stress only modifies the circulation in the upper ocean. However, it is noticeable that wind stress can play a vitally important role in determining the location and strength of the meridional overturning in global ocean circulation models [e.g., *Toggweiler and Samuels,* 1993; *England,* 1993]. In fact, as will be discussed in the next section, the wind-driven circulation in the oceans plays an important role in determining the position of the saline cell in the upper ocean which affects the location of deep water formation and sinking.

Table 1. Competition Between Forcings of the Thermohaline Circulation: Freshwater Flux, Heat Flux, and Wind Stress

Case	$E-P$, m yr^{-1}	Thermal Forcing	Integration Time, years	Mean Kinetic Energy, erg cm^{-3}	Heat Flux, 10^{15} W	$\overline{S}_s$, psu	$\overline{T}$, °C	M_m, Sv
F	0.5	···	1369	0.3051	···	−0.717	···	−85.84
T	0.0	1.0	2191	0.2420	0.344	···	2.709	25.70
TF	0.5	1.0	2191	0.1036	0.279	0.970	3.233	22.70
WTF-1	0.5	1.0	4383	0.4880	0.477	0.479	3.618	23.70

$\overline{S}_s$ is the basin mean surface salinity (deviation from the mean of 35 psu), $\overline{T}$ is the basin mean temperature, and M_m is the strength of meridional overturning.

In the past, a buoyancy formulation has been used extensively to study the thermohaline circulation. Assuming that both the thermal forcing and saline forcing can be parameterized in terms of the relaxation conditions with the same relaxation coefficient and that the equation of state is linear,

$$\rho = \rho_0(-\alpha T + \beta S)$$

then the effects of the thermal and saline forcings can be combined into a single buoyancy flux, defined by

$$F_\rho = -\rho(\alpha F_T - \beta F_S)$$

This buoyancy flux may not be used directly to determine the direction of the meridional overturning forced by the combined thermal forcing and saline forcing.

As an example, let us compare the contributions from these two forcings. Since the total heat flux from the ocean to the atmosphere, calculated from case T, is 0.279×10^{15} W, the buoyancy flux due to thermal forcing is

$$\frac{\alpha Q}{C_p} = 1.6 \times 10^{-4} \times 0.279 \times 10^{15} \times 0.239 = 1.07 \times 10^{10} \text{g s}^{-1}$$

The total amount of freshwater flux, calculated from case F, is 0.156×10^{12} cm^3 s^{-1}; the contribution due to evaporation minus precipitation is

$$\rho\beta\overline{S}(E-P)A = 35.97 \times 7.71 \times 10^{-4} \times 0.158 \times 10^{12} = 0.44 \times 10^{10} \text{g s}^{-1}$$

These two numbers give no indication of the strength of the meridional circulation induced by these forcings. Such a formulation does not apply exactly to the model with the natural freshwater flux boundary condition for salinity. In fact, the meridional overturning of the saline circulation driven by the freshwater flux alone is 3 times that driven by the thermal forcing alone. This difference is due to the nature of the freshwater flux forcing in contrast to that of the thermal forcing. In fact, it has been shown that the strength of the saline circulation is proportional to the one-fourth power of the freshwater flux, while the strength of the thermal circulation is proportional to the cubic root of the meridional temperature difference [*Huang and Chou,* 1994].

As will be shown shortly, a slight increase (from 0.5 m yr^{-1}) in the freshwater flux will induce the collapse of the thermal mode and the establishment of the saline mode, so that the buoyancy formulation is not an accurate indicator for comparing the strength of the thermohaline forcing.

4. Thermohaline Circulation Without Wind Stress

The first set of experiments is purely thermohaline circulation forced by temperature relaxation and freshwater flux (Table 1). In experiment TF-1, the freshwater flux is relatively weak, $W_0 = 0.5$ m yr^{-1}. Starting from an initially homogeneous state, the model ocean reaches a stable state within 1000 years. This state is a thermal mode, with sinking in the north and upwelling elsewhere. The upper ocean is covered by relatively salty water which is typical of the thermal mode.

As the freshwater flux is increased to $W_0 = 0.7$ m yr^{-1}, the model exhibits flushing with a quasi-period of 1000 years. As discussed in section 1, the thermal relaxation time is much shorter than the saline relaxation time; thus the thermohaline circulation is thermally controlled at the initial stage. At year 28, the first peak of meridional overturning with sinking in the north is established. Although an oscillation sets in, over the first 200 years the mean sea surface salinity (deviation from 35 psu) keeps increasing and the basin mean temperature keeps declining; these two indexes indicate that a thermal mode of thermohaline circulation is gradually established.

However, this thermal mode of circulation is not stable; after 200 years, the freshwater flux forcing gradually takes over. The mean sea surface salinity (deviation from 35 psu) becomes negative at year 261, indicating a transition from the thermal mode to the saline mode. Between years 261 and 900, the saline mode is gradually set up. The saline mode is characterized by a shallow and weak indirect cell in the upper ocean, whose strength is about 2.5 Sv for a snapshot taken at year 1644 (Figure 2a). This is much smaller than the sinking rate of 100 Sv for a pure saline mode driven by the same amount of freshwater flux alone [*Huang and Chou,* 1994]. Water below the upper kilometer is basically stagnant. The slow meridional circulation is associated with a relatively large meridional salinity gradient which is the controlling factor in driving the meridional circulation. Because the circulation is sluggish, the surface salinity drops below 31 psu along the northern boundary of the basin. The sluggishness of the meridional circulation and the freshness of the upper ocean are typical of the saline mode circulation. Notice that there is a very thin and sharp halocline in the upper ocean for the purely saline circulation [*Huang,* 1993]. However, the saline mode in the present case is quite different because there is not such a sharp halocline. Instead, the entire northern basin is fresh.

It is important to notice that the basin mean temperature increases during the establishment of the saline mode because of the relatively warm water sinking at low latitudes. Water sinking at low latitude is not dense enough to sink all the way to the bottom because it is quite warm. Within 600 years, the abyssal water gradually warms up and becomes saltier, and this sets up the prestage of the violent flushing. A typical snapshot of the circulation during the flushing is shown in Figure 2b; there is a violent overturning at the northeastern corner and basin-wide upwelling. During the flushing phase the circulation is a transitional thermal

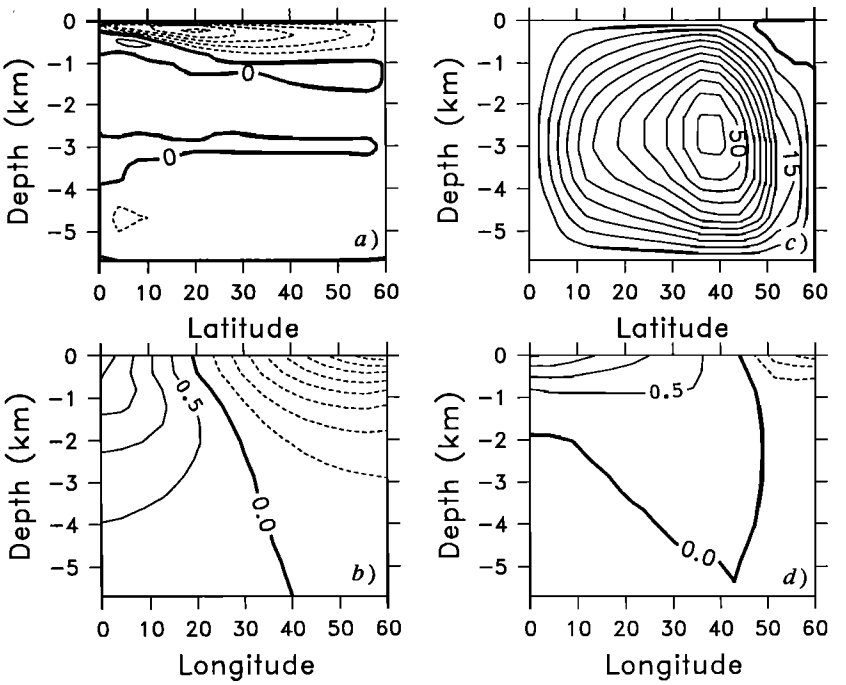

Figure 2. Instantaneous structure of the circulation, case TF-2. The meridional overturning streamfunction (in Sverdrups) at (a) 1644 yr and (b) 1096 yr; (c) the zonal mean salinity at 1644 yr and (d) at 1096 yr.

mode, characterized by the relatively salty water in the upper ocean (Figure 2d).

In the third experiment, the freshwater flux amplitude is increased to 1 m yr^{-1}. Since the freshwater flux is working against the thermal forcing, the first peak of the meridional overturning is postponed from year 28 to year 34, while the setup of the saline mode is advanced from year 261 to year 157. Notice that the flushing period is reduced from 1000 years to 710 years (Figure 3). The relation between the amplitude of freshwater flux

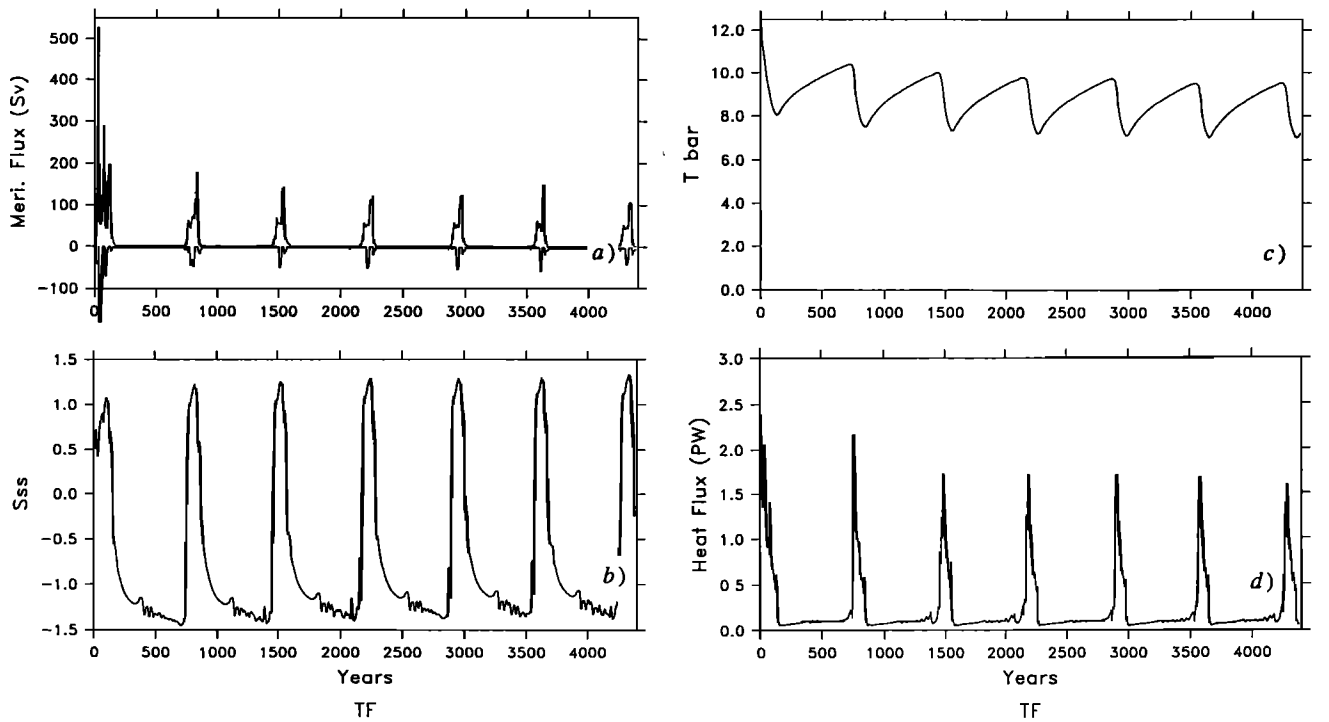

Figure 3. Time evolution of the model forced by heat flux and freshwater flux, case TF-3, the amplitude of $E - P$ is 1.0 m yr^{-1}. (a) The strength of the meridional overturning cell; (b) the mean sea surface salinity (deviation from the basin mean), in practical salinity units; (c) the basin average temperature, in degrees Celcius; and (d) the heat loss to the atmosphere, in 10^{15} W.

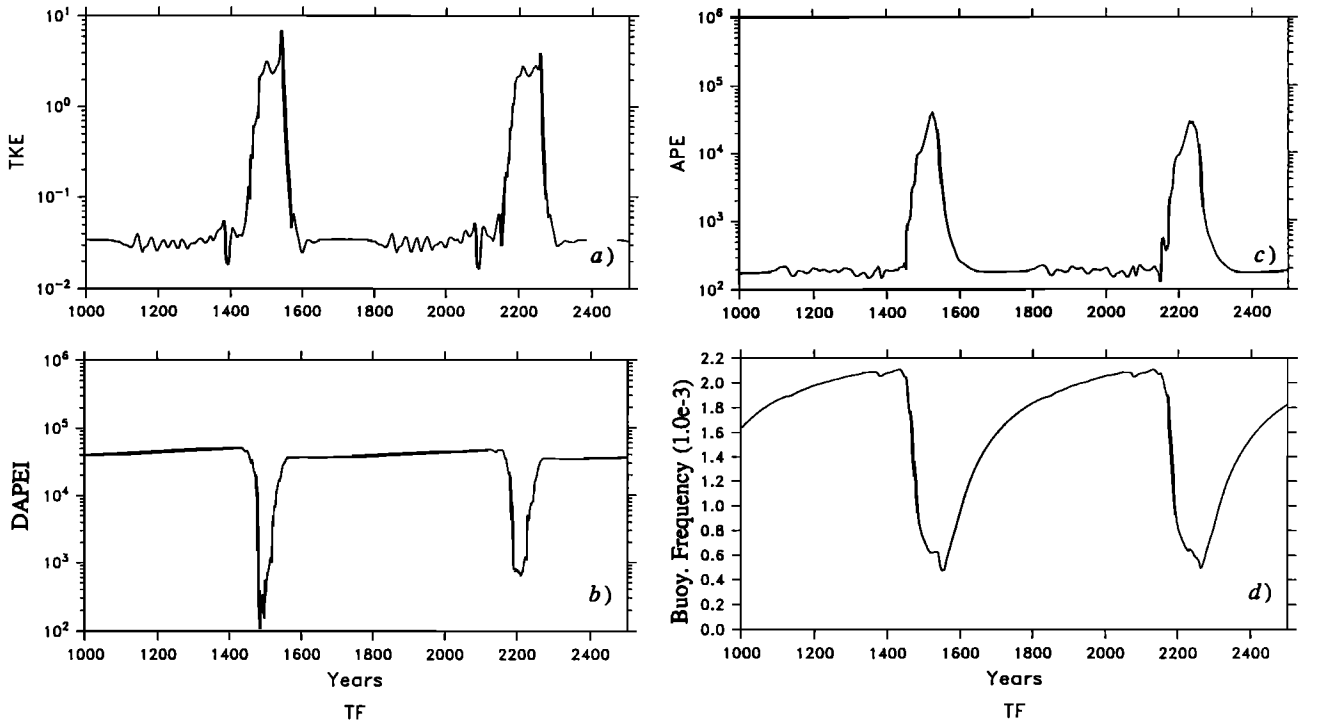

Figure 4. Time evolution of the model, case TF-3, all energy densities in ergs per cubic centimeter. (a) The mean kinetic energy; (b) the diabatic available potential energy index (DAPEI); (c) the available potential energy (APE); and (d) the mean buoyancy frequency in the upper ocean of the northern basin, in cycles per second.

and the period of flushing is unclear because, as will be shown in the next section, an increase of freshwater flux will increase the period of flushing for a model forced by wind stress, thermal forcing, and freshwater flux.

The energetic flushing is supported by a rapid release of potential energy associated with the potentially unstable stratification of the saline mode [*Marotzke,* 1989; *Wright and Stocker,* 1991]. As discussed in the appendix, the saline mode is characterized by cold and relatively fresh water overlying warm and salty abyssal water. Thermohaline circulation forced by freshwater flux is usually associated with fluctuations; even the explicit convective adjustment itself is a continuous source of perturbations. Such small perturbations can lead to strong convective instability in the following way. Because the relaxation time for temperature is much shorter than that for salinity, as the warm and salty deep water is brought to the surface, it will be quickly cooled down by the cold atmosphere at high latitudes, while maintaining its salinity. As a result, the water column becomes gravitationally unstable; overturning takes place and the potential energy released during the convective overturning provides energy supporting the convective overturning. Since this process is self-energized, once it begins it will keep going until a large part of the energy source is consumed.

A typical example of energetics between two flushings is shown in Figure 4. During the first phase of a flushing period, both the mean kinetic energy and the available potential energy (APE) are increased 100 times, while the DAPEI declines at least 100 times. Therefore, it is clear that the energy source supporting the flushing is not from the APE, and it must come from the DAPEI. In fact, during the flushing period a big meridional temperature gradient due to the strong cooling in the northern basin gives rise to a rapid increase of APE.

To explore whether the weakening of the stratification in the northern basin may serve as a precondition for the flushing, the mean buoyancy frequency of the deep water (below 537 m) is averaged over the northern half of the basin. From Figure 4d, it is seen that the stratification is substantially weakened during the flushing but it is reestablished after the flushing. In fact, the mean stratification reaches a maximum just before a flushing starts. Therefore the weakening of the stratification is not a necessary precondition for the flushing. The most important factor that sustains the flushing is the release of the DAPEI associated with the cold and relatively fresh water overlying the warm and salty water below.

5. Combined Wind-Driven and Thermohaline Circulation

In the second set of numerical experiments wind stress is added. Each experiment is spun-up from an initially homogeneous ocean. In the first experiment, the freshwater flux amplitude is 0.5 m yr^{-1}. After

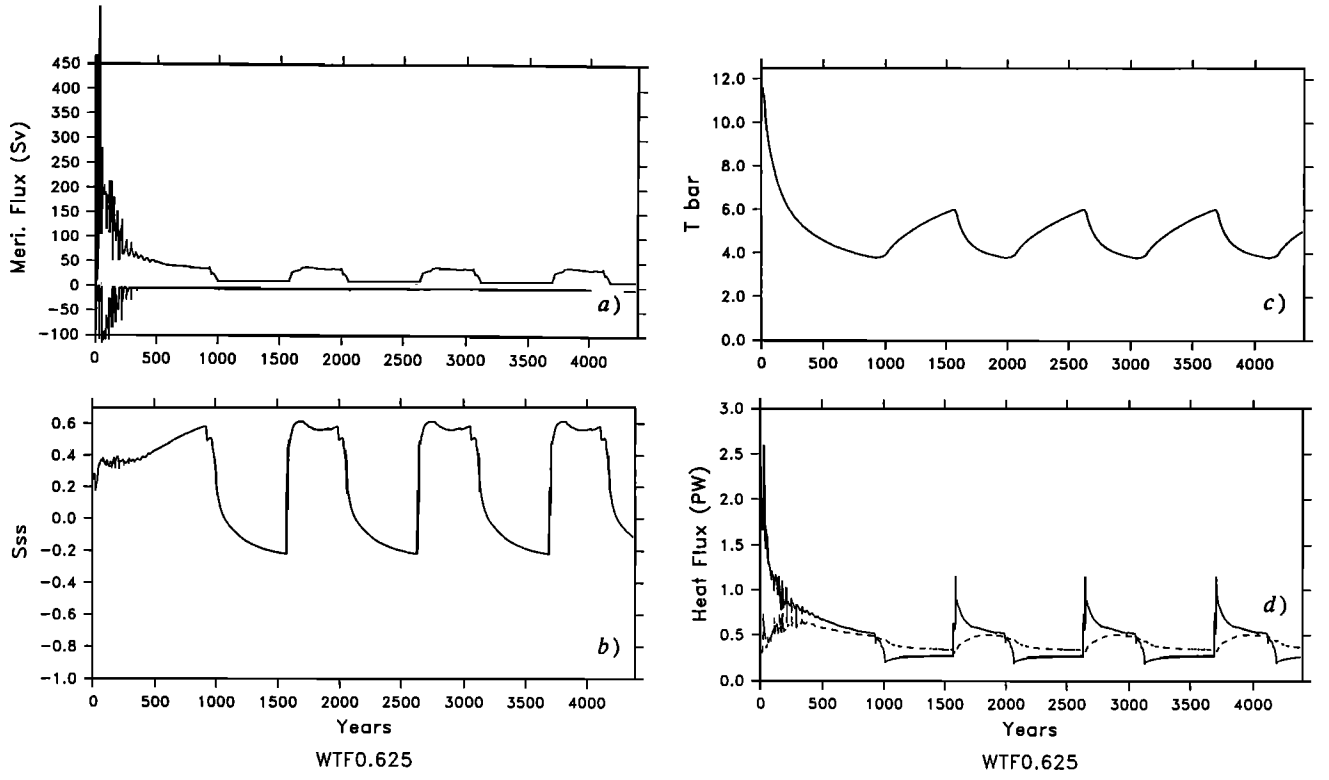

Figure 5. Time evolution of the model, case WTF-3, the amplitude of $E - P$ is 0.625 m yr^{-1}. See text explanation of Figure 2.

1000 years, a thermal mode is well established. Although there is a sudden drop in the surface salinity at year 1300, the circulation remains in the thermal mode, characterized by sinking along the northern boundary and upwelling elsewhere. Compared with the case of no wind stress, the present case is slightly different because there is a very thin layer of southward motion in the upper ocean of the northern basin due to the Ekman flux under the westerly winds. This southward moving layer, combined with the precipitation in the subpolar basin, gives rise to a thin halocline in the subpolar basin. As will be shown shortly, the existence of the halocline is a very important component of the combined wind-driven and thermohaline circulation. Except for the thin saline cell on top of the subpolar basin, the meridional circulation is typical of a thermal mode, with sinking taking place at the northeastern corner.

As the freshwater flux amplitude is increased to 0.625 m yr^{-1}, the model ocean enters a supercritical state, in which the thermohaline circulation does not reach a single steady state (Figure 5). Instead, the model is in a continuous transition between a quasi-steady saline mode and a very unsteady thermal mode (the flushing mode). Similar to the cases of purely thermohaline circulation, a thermal mode is first established soon after the spin-up process is started. However, the freshwater flux forcing works against the thermal forcing, so the increase in the freshwater flux postpones the time of the first maximum in the meridional overturning, but it accelerates the establishment of the saline mode, as seen from the last two columns in Table 2.

As the amplitude of the freshwater flux is increased, the period of flushing also increases from 1000 years to 6000 years. The timescale of flushing is determined by the diffusion time for the abyssal water to be warmed up and become salty. The following discussion will concentrate on a pivotal case which is forced by a freshwater flux of 1 m yr^{-1}. As seen from Figure 6, the model flushes with a quasi-period of 6000 years. Each flushing is slightly different from the others, and there are decadal oscillations between big flushings, typical for saline-dominated circulation. Such decadal oscillations can be explained in terms of the Howard–Malkus loop oscillator [*Welander*, 1986; *Weaver et al.*, 1991; *Winton and Sarachik*, 1993]. Since the present model is based on a no-salt flux condition for the salinity, the explanation of decadal oscillations is more straightforward. Because there is no salt flux across the air–sea interface, any salinity perturbations would be carried downstream by the meridional overturning cell and appear repeatedly. In addition, there is a negative feedback between the local salinity and the meridional overturning. If there is a negative surface salinity anomaly along the southern edge, the meridional pressure gradient associated with the salinity difference declines. As a result, the meridional circulation slows down. A slow meridional circulation means water in the southern basin is exposed to evaporation for longer time. Thus the sur-

Table 2. Dependence of Thermohaline Catastrophe on the Amplitude of the Freshwater Flux

Case	$E-P$ Amplitude, m yr^{-1}	Integration Time, years	Flushing Period, years	First Meridional Flux Maximum, years	First Time $\overline{S}_s = 0$, years
TF-1	0.5	2191	...	...	...
TF-2	0.7	2191	1000	28.1	261.4
TF-3	1.0	4383	710	33.86	157.3
WTF-1	0.5	4383	...	...	...
WTF-2	0.6	4383	...	...	...
WTF-3	0.625	4383	1000	30.9	1075.5
WTF-4	0.65	4383	1500	31.6	1001.4
WTF-5	0.7	7671	3000	33.3	840.1
WTF-6	1.0	32329	6000	37.6	271.6

face salinity in the southern basin increases. Owing to the inertia of the system, the surface salinity at low latitudes can overshoot the equilibrium value, and the second half of the salt oscillation is under way. Thus the salt oscillation cycle is due to such a conveyor.

A typical flushing can consist of several peaks in the meridional overturning and zonal overturning which have a time scale of about 50 years. For example, during the second flushing (year 12,070–12,400) there are seven peaks in the meridional flux (Figure 7a). During the first peak in the meridional overturning (about year 12,100), there is also a sharp increase in heat flux (Figure 7b).

The energy diagnosis during a flushing is shown in Figure 8. There are also several peaks in each figure. The first peak in total kinetic energy (TKE) is around year 12,100. Notice that APE increases during the same period, but there is a sharp decline in the DAPEI (Figures 8b and 8c). Therefore, it is clear that this first peak in the kinetic energy has its source from the DAPEI, not from the APE. However, the other six peaks in the mean kinetic energy are associated with the decline in the APE, while the DAPEI is gradually increased (except for a sharp drop near year 12,340). Thus the kinetic energy conversion from APE seems to contribute to the overturning during these periods. Notice that

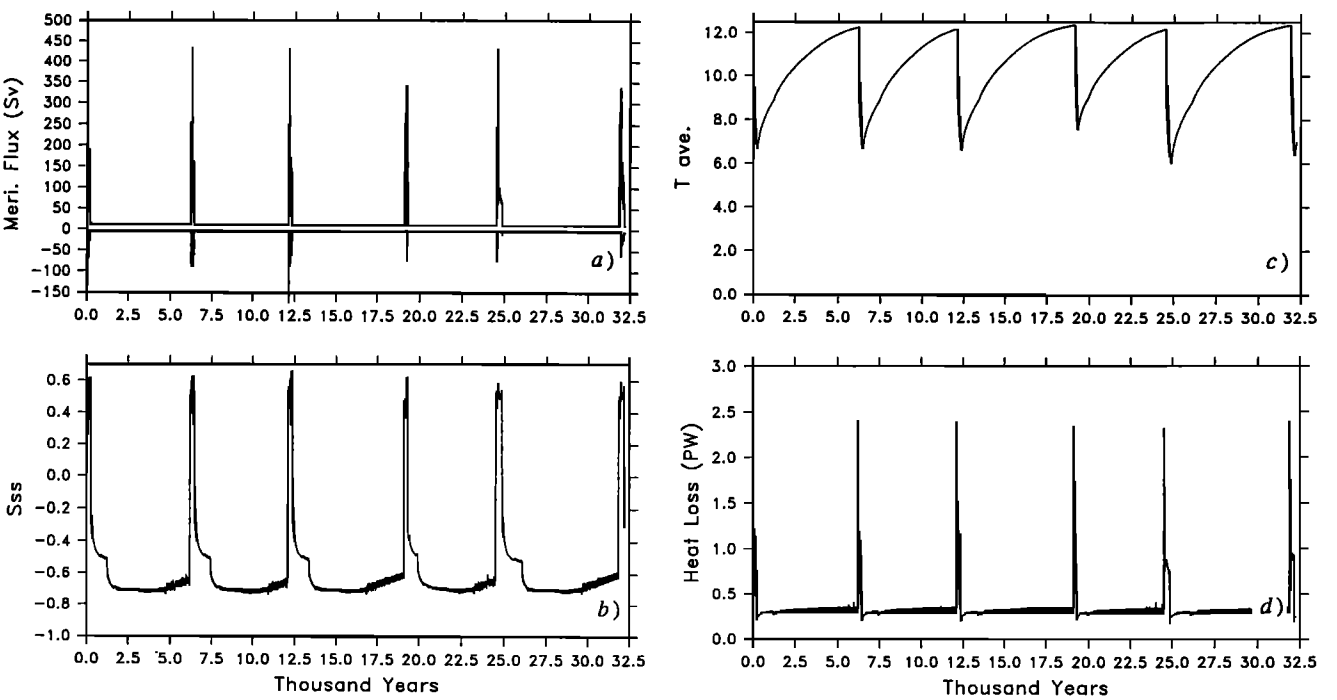

Figure 6. Time evolution of the model, case WTF-6, the amplitude of $E-P$ is 1.0 m yr^{-1}. See text explanation of Figure 2.

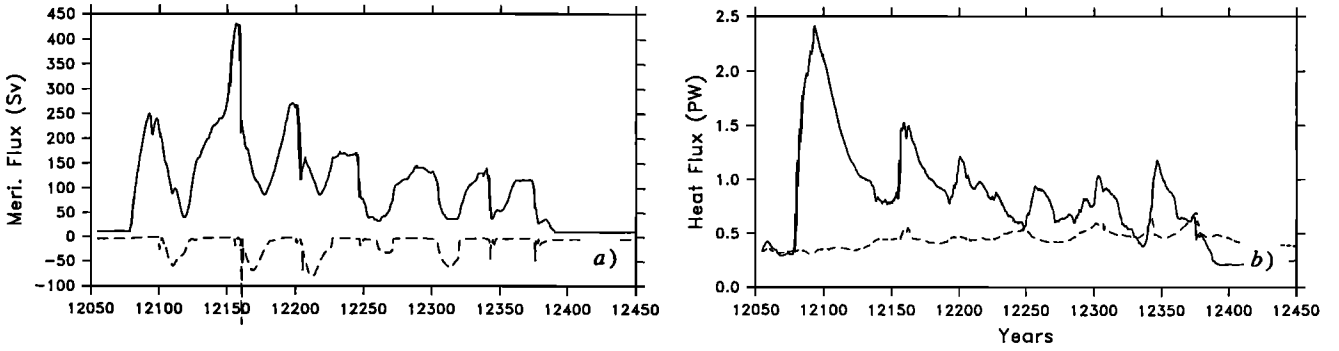

Figure 7. Time evolution of the solution during a flushing, case WTF-6. (a) The strength of the meridional overturning cell, the solid line indicates the direct cell (sinking in the north) and the dashed line indicates the indirect cell (sinking in the south); (b) the heat loss to the atmosphere (solid line) and heat gain from the atmosphere (dashed line), in 10^{15} W.

the peaks of TKE are no larger than 40 units, while the peaks in DAPEI and APE are 10^5 times larger. Thus the conversion rate from APE to TKE or from DAPEI to APE is very low, no more than 0.1%. Apparently, the major portion of the energy is lost to mixing and dissipation. During the flushing period, the mean buoyancy frequency averaged over the northern deep ocean is first reduced sharply, then gradually reestablished.

Between two flushings, the abyssal water is gradually warmed up, so the DAPEI is gradually increased, while the stratification of the abyssal water is substantially reduced during this long period when the deep ocean is gradually warmed up (Figure 9). A thousand years after the first flushing the ocean is restratified, and the mean stratification of the abyssal water in the northern basin can reach 1.7×10^{-3} c s^{-1}. However, as the deep water is gradually warmed up through diffusion, the mean stratification of the abyssal water in the northern basin is gradually reduced to about 1.0×10^{-3} c s^{-1} just before the second flushing starts at year 12,070. As the deep water is warmed up through diffusion, the vertical temperature gradient in the northern basin is increased. Accordingly, the DAPEI is increased from 2×10^4 erg cm^{-3} to 1×10^5 erg cm^{-3}.

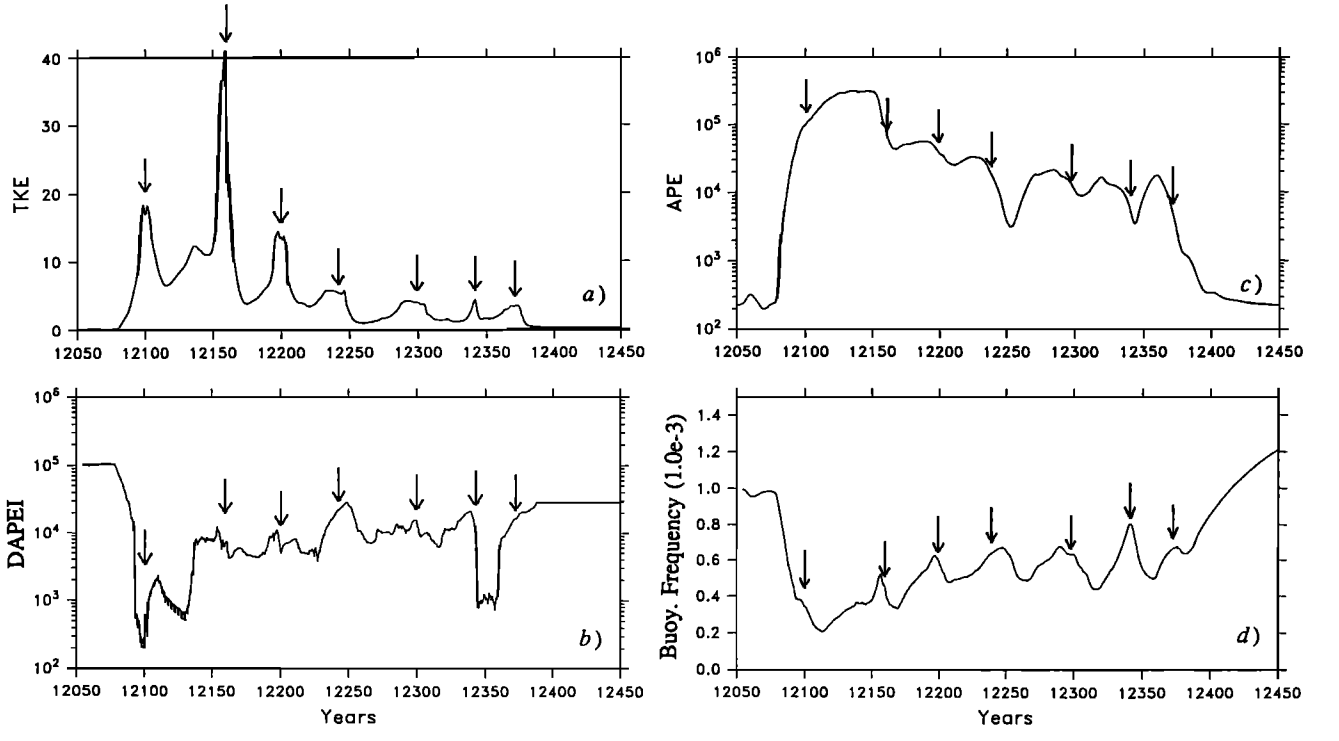

Figure 8. Time evolution of the model during a flushing, seven arrows indicate individual peaks in the meridional overturning cell, all energy densities in ergs per cubic centimeter. (a) The mean kinetic energy; (b) the diabatic available potential energy index (DAPEI); (c) the available potential energy (APE); and (d) the mean buoyancy frequency in the upper ocean of the northern basin, in cycles per second.

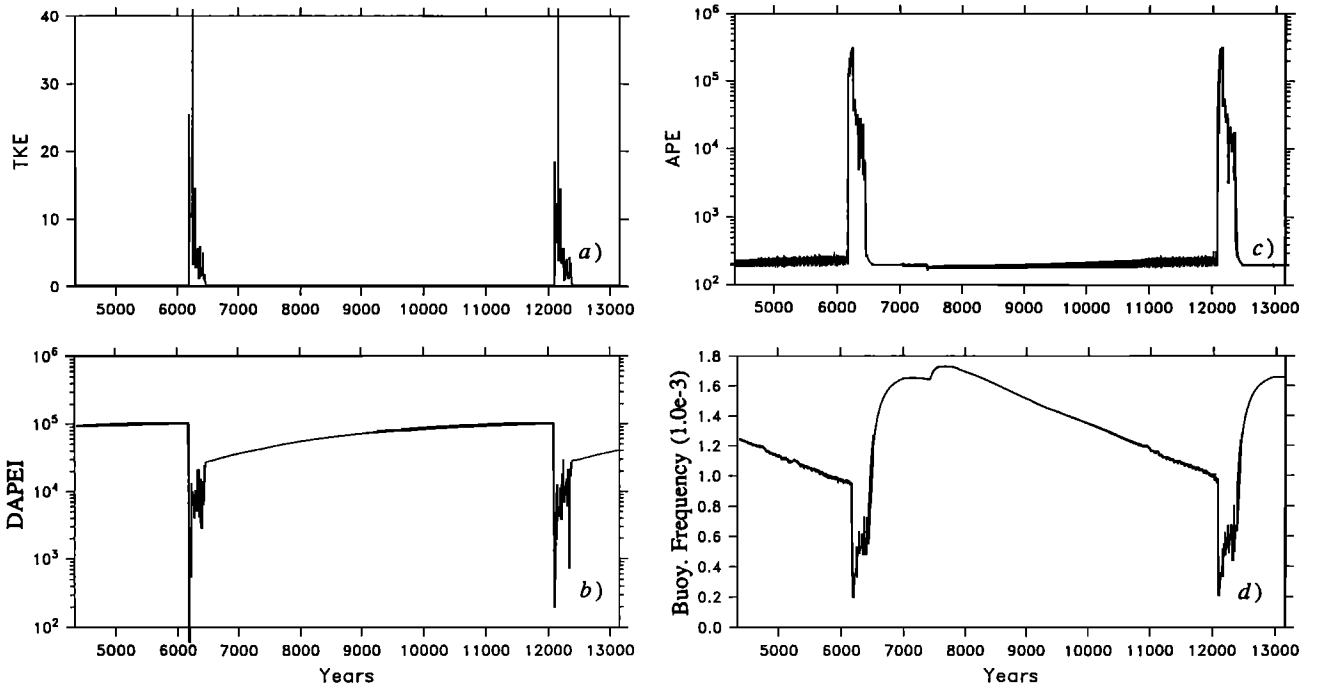

Figure 9. Time evolution of the model between two flushings, case WTF-6; see caption for Figure 4.

Similar to the cases of no wind stress, the model ocean remains in the quasi-saline mode for most of the time. The saline mode is characterized by a slow and shallow meridional circulation. There is a saline cell in the northern basin with a mass flux of about 4.8 Sv and a thermal cell in the southern basin with a mass flux of 10.6 Sv (Figure 10a). It is speculated that when the freshwater flux is very strong the circulation may be entirely saline-dominated so that the saline cell would cover the whole basin. The existence of the direct thermal cell in the subtropical basin is probably due to the Ekman drift associated with the easterly wind at the low latitudes and the northward western boundary current of the subtropical gyre, which prevents the saline cell from invading the southern basin.

As a result of the competition between all forcings,

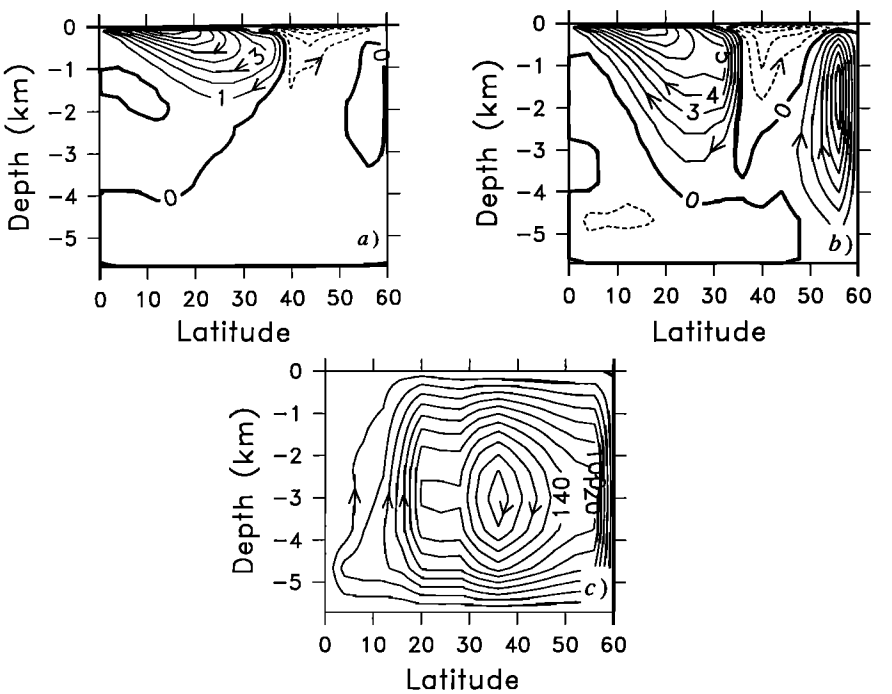

Figure 10. Instantaneous structure of the meridional circulation for case WTF-6, (a) at year 9185; (b) year 12,078, and (c) year 12,098.

water sinks at midlatitude. Since such water is not very cold, it cannot sink all the way to the bottom; instead, sinking water only goes to about 2 km. Thus these two cells are surface trapped and there is intermediate water formation at midlatitude.

The intermediate water formed in the present model is due to the Ekman convergence at middle latitudes. One should notice that the intermediate water formation in the world oceans is a much more complicated phenomenon. Recently, *England* [1992, 1993] and *England et al.* [1993] have carried out a series of numerical experiments for water mass formation in the world oceans. These numerical experiments demonstrated that in order to simulate the intermediate water formation, such as the Antarctic Intermediate Water and the North Pacific Intermediate Water, it is of vital importance to use realistic topography and realistic thermohaline boundary conditions on the upper surface, including the seasonal cycle.

In comparison with the saline mode, the thermal mode is a very short and energetic episode. During the initial phase of flushing, a direct cell near the northern boundary grows very fast through energy release by strong cooling (Figure 10b). This direct cell eventually spreads to the whole basin (Figure 10c).

The location of the downward branch of the thermohaline circulation shifts during different phases of the transition. When the model is in the saline mode phase, intermediate water is formed at midlatitude, both in the western boundary region and in the ocean interior (Figure 11a). At the beginning of flushing, deep water starts to be formed at the northwestern corner (Figure 11b). During most of the flushing phase, much of the deep water is actually formed in the northeastern basin, which is typical of the thermal mode.

All results discussed above are based on the natural boundary conditions for the salinity. A comparison run based on the virtual salt flux (the old models) has been carried out. A major difference between these two cases is the flushing period. Flushing happens more frequently in the old model than in the new model. For example, the first flushing begins at year 5770 and ends

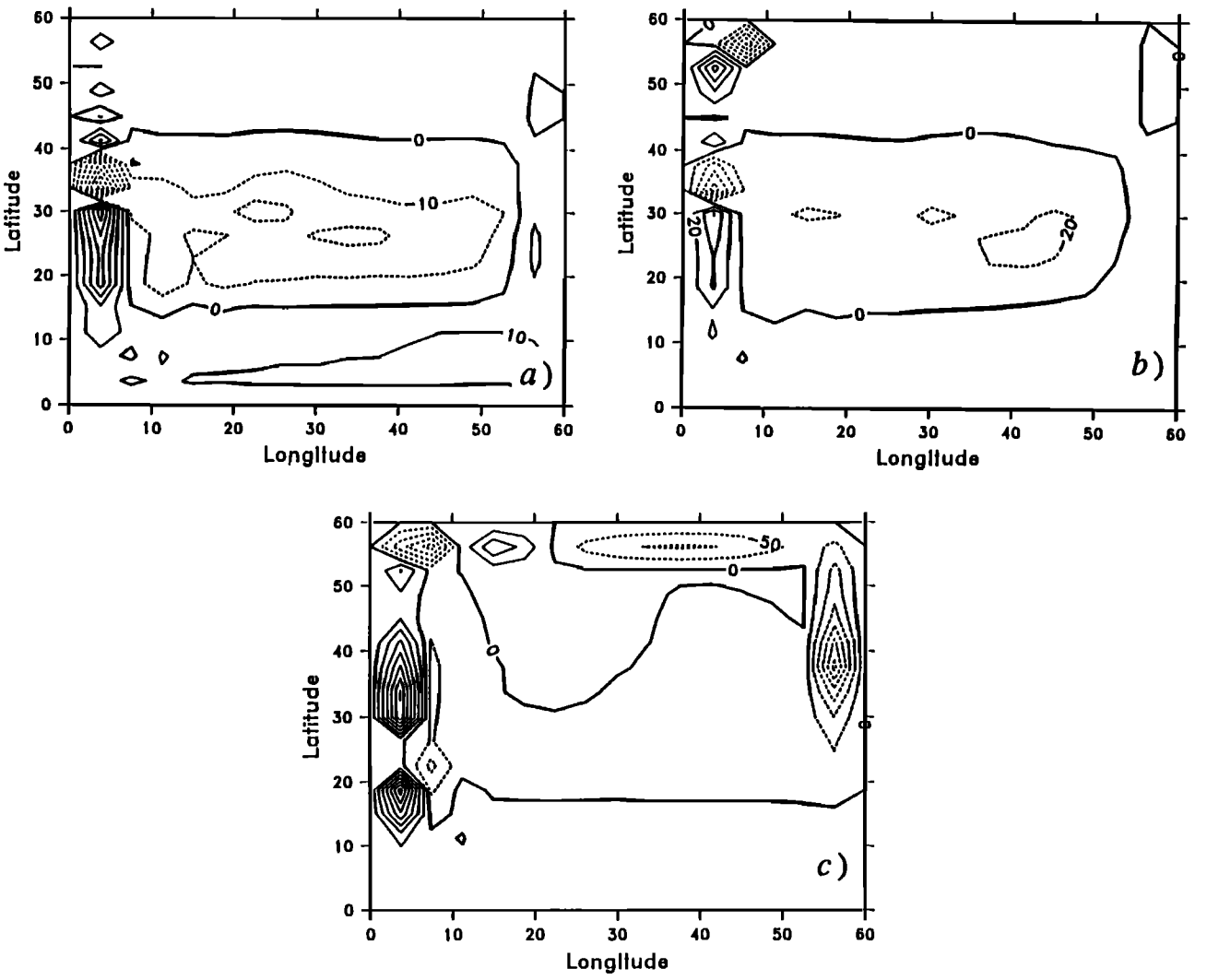

Figure 11. Vertical velocity maps (at z = 191 m, in 10^{-5} cm s^{-1}) at (a) year 9,185; (b) year 12,078; and (c) year 12,098.

at year 6087 in the old model, while in the new model it happens between year 6173 and year 6466. Integration over long time periods of the old model shows that the average flushing period is about 10% shorter than that of the new model. During the first part of the flushing these two models behave rather similarly; however, at the end of the flushing, the new model exhibits a few more oscillations than the old model.

6. Discussion

The amplitude of freshwater flux is a very important parameter in determining the basic structure of the thermohaline circulation. When the freshwater flux amplitude is subcritical, the thermohaline circulation appears in a stable thermal mode, characterized by sinking in the north and a lack of variability. The thermal mode circulates relatively fast, with a mass flux of more than 20 Sv, and the upper ocean is relatively salty. For the case with wind stress, there is a very shallow halocline in the upper ocean of the subpolar basin driven by the westerlies.

When the freshwater flux is supercritical, the thermohaline circulation can never reach a single steady state; instead, the model ocean is in a continuous transition between a quasi-steady saline mode and a very unsteady thermal mode. The thermal mode phase is relatively short, about several decades, while the saline mode phase is quite long, on the order of thousands of years. The short life of the thermal mode is related to the short relaxation time associated with the upper boundary condition for the temperature. The longevity of the saline mode is due to the long relaxation time associated with the upper boundary condition for the salinity and the long diffusion time for the deep water to become warm and salty.

The quasi-steady saline mode is characterized by slow and shallow meridional circulation and intermediate water formation (water is not cold enough to sink to the bottom). For the cases of no wind stress, the saline mode is characterized by sinking along the equator and basinwide upwelling. For the cases with wind stress, the saline mode is characterized by an indirect, saline cell in the subpolar basin and a direct, thermal cell in the subtropical basin. Both cells are shallow and they circulate slowly, especially the saline cell. The combination of these two cells forces water to sink at midlatitude.

The saline mode is always associated with perturbations. During the saline mode phase, the deep water gradually becomes warm and salty. Thus at the end of the saline mode phase, there is cold and relatively fresh water lying on top of warm and salty water, and such a vertical structure is potentially very unstable. Small perturbations can grow by the release of the diabatic available potential energy index. Thus a final equilibrium in the saline mode cannot be reached; instead, the model ocean flips to a very energetic thermal mode in which violent overturning fed by the DAPEI destroys the vertical stratification. After the potentially available energy is consumed, the model ocean returns to the saline mode and the whole cycle will be repeated again.

The structure of the thermohaline circulation in the supercritical state has been discussed in many previous studies such as those by *Marotzke* [1989] and *Weaver and Sarachik* [1991]. The inclusion of wind stress seems to be an important factor controlling the location of intermediate water formation. In a 3 × 2 box model [*Huang et al.*, 1992], it has been demonstrated that intermediate water formation at midlatitude requires a nonlinear $E - P$ profile, with strong evaporation at subtropical latitudes. However, in a three-dimensional model with wind stress, the easterlies at low latitude prevent the saline cell from invading the subtropical basin that leads to intermediate water formation at midlatitude.

The steady thermal mode for the subcritical state resembles the thermohaline circulation in the present North Atlantic. The early stage of the saline mode for the supercritical state, especially the intermediate water formation at midlatitude, resembles the thermohaline circulation in the North Pacific, as described by *Reid* [1965]. Notice that in the world oceans, cold bottom water formed along Antarctica dominates. Thus the potentially unstable situation of cold and fresh water lying on top of warm and salty water does not exist in the present-day oceans. However, if the bottom water formation around the Antarctica were interrupted, could such an unstable situation occur?

The present study emphasizes that the essential difference between the thermohaline circulation in the North Atlantic and in the North Pacific may be the amount of evaporation and precipitation. In the present North Atlantic, the precipitation (minus evaporation) rate is no more than 0.5 m yr^{-1}, which is lower than the critical value of about 0.6 m yr^{-1} found in this study. If the precipitation rate is increased, the thermohaline circulation in the North Atlantic may switch to the saline mode, which is characterized by intermediate water formation at midlatitude. Such a mode of operation did exist during the last glaciation, as discussed by *Duplessy et al.* [1988]. Similarly, if the evaporation and precipitation rates in the North Pacific are substantially reduced, its circulation may switch back to the thermal mode.

Although the present model is highly idealized, the results from the model are consistent with many previous studies in pointing out the possible collapse of the thermal-dominated circulation in the North Atlantic if the freshwater flux is slightly increased [e.g., *Maier-Reimer and Mikolajewicz*, 1989]. Note that the critical value of freshwater flux required from such a transition in the present model is substantially lower than that in the model by *Winton and Sarachik* [1993]. The high value of the critical freshwater flux required in the Winton and Sarachik model may be due to the frictional

geostrophy and upper boundary conditions used in their model. As demonstrated in many previous studies [e.g., *Weaver and Sarachik,* 1991; *Weaver et al.,* 1991, 1993; *England,* 1992, 1993; *Moore and Reason,* 1993; *Huang,* 1993], the thermohaline circulation and its variability are very sensitive to the upper boundary conditions, especially the freshwater flux (or the virtual salt flux in many old models); further study based on more realistic geometry and surface boundary conditions is required for better understanding of these issues.

Appendix: Diabatic Available Potential Energy Index

The saline mode is characterized by cold and relatively fresh water lying on top of warm and salty water. Although the state is adiabatically stable, it is potentially very unstable during a diabatic process because potential energy can be released through overturning and cooling.

The basic idea can be demonstrated by a very simple box model as follows (Figure A1): Assuming a two-box model with salinity S_1 and S_2 and temperature T_1 and T_2, the equation of state is in a linear form

$$\rho = \rho_0(1 - \alpha T + \beta S)$$

The total potential energy (per unit area) for the initial state is

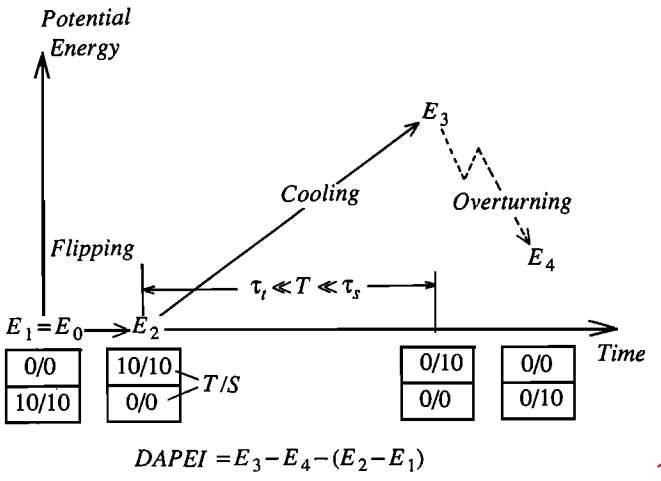

Figure A1. Schematic diagram illustrating the meaning of diabatic available potential energy index (DAPEI) released during the flipping–cooling–overturning process. For convenience, assume $\alpha = \beta = 1$ and T, S, and energy are in nondimensional units. The model consists of two vertical boxes, and the numbers m/n in each box indicate the temperature and salinity. The essential assumption is that the timescale of the second phase is much shorter than the relaxation time for the salinity, but much longer than the relaxation time for temperature. Thus the model's temperature changes during the second phase, but the salinity remains unchanged.

$$E_1 = \frac{gh^2}{2}(3\rho_1 + \rho_2)$$
$$= E^0 + \frac{\rho_0 g h^2}{2}[-\alpha(3T_1 + T_2) + \beta(3S_1 + S_2)],$$

where $E^0 = 2\rho_0 g h^2$ is a constant.

Flipping. If water in these two boxes is exchanged vertically, the total potential energy for the new state is

$$E_2 = E^0 + \frac{\rho_0 g h^2}{2}[-\alpha(T_1 + 3T_2) + \beta(S_1 + 3S_2)]$$

Assuming that the initial state is gravitationally stable, then energy required for this vertical exchange is

$$\Delta E_2 = \rho_0 g h^2 [-\alpha(T_2 - T_1) + \beta(S_2 - S_1)]$$

Cooling down. State 2 is characterized by warm water in the upper box which is exposed to the cooling of the atmosphere. The temperature relaxation time τ_t is on the order of a month, while the salinity relaxation time τ_s is much longer, on the order of a decade. Thus for a time which is much longer than τ_t but much shorter than τ_s, the model is transferred to state 3 in which upper layer temperature is reduced to T_1, while the salinity is unchanged. The corresponding potential energy is

$$E_3 = E^0 + \frac{\rho_0 g h^2}{2}[-\alpha(T_1 + 3T_1) + \beta(S_1 + 3S_2)]$$

State 3 is gravitationally unstable and overturns to state 4 whose energy is

$$E_4 = E^0 + \frac{\rho_0 g h^2}{2}[-\alpha(T_1 + 3T_1) + \beta(3S_1 + S_2)]$$

During the transition from state 3 to 4, a large amount of potential energy is released. The diabatic available potential energy index (DAPEI) is defined as the energy released during the overturning minus the energy required to push the slightly heavy water from the lower box upward to initiate the whole process,

$$DAPEI = E_4 - E_3 - (E_2 - E_1) = \rho_0 g h^2 \alpha (T_2 - T_1)$$

Notice that the definition of the DAPEI does not include the salinity explicitly. Nevertheless, the salty water in the bottom box is a precondition for the convective instability. Most of the potential energy released during the convective overturning is lost to violent vertical mixing, and only a very small part (less than 0.1%) of this energy is converted into kinetic energy of large-scale motions. Therefore, we use the name diabatic available potential energy index to indicate the subtle difference between the classical definition of available potential energy (APE) and the quantity defined in this study.

For the continuously stratified ocean, we propose a generalized definition. Assuming both temperature and salinity increase downward, one can repeat the same

argument for a continuously stratified water column. First, notice that one essential element involved in the definition of DAPEI is the fast removal of thermal anomaly by air–sea interaction. The rapid release of the potential energy is associated with water mass exchange between the surface layer and subsurface layer. Thus although convective overturning can take place between subsurface layers, the contribution to the DAPEI is primarily due to convective overturning started from the surface. Second, convective overturning is very close to a one-dimensional phenomenon in our low-resolution model, so we extend our one-dimensional argument into a definition of DAPEI for a three-dimensional ocean

$$DAPEI = \int\int\int_0^H g\rho_0\alpha\,[T(z) - T_{\text{surf}}]\,(H - z)\delta\,dzdxdy$$

where δ is a switch, $\delta = 1$ if $T(z) > T_s$ and $S(z) > S_s$, and $\delta = 0$ otherwise. Thus the switch δ is on only if the stratification is in favor of convective overturning.

In comparison, the classic APE is defined as

$$APE = \int\int\int -\frac{g\rho'^2}{2}\left(\frac{\partial\overline{\rho}}{\partial z}\right)^{-1} dxdydz,$$

where $\partial\overline{\rho}/\partial z$ is the horizontal mean of the vertical density gradient.

Acknowledgments. Most of the calculations were carried out on the CRAY-YMP at the Geophysical Fluid Dynamics Laboratory at Princeton, many thanks to G. Philander and K. Bryan. Two reviewers' comments helped to improve the text. This study was partially supported by the National Science Foundation through grant OCE 90-17158. This is contribution 8275 from the Woods Hole Oceanographic Institution.

References

Bryan, F., High-latitude salinity effects and interhemispheric thermohaline circulations, *Nature, 323,* 301–304, 1986.

Bryan, K., A numerical method for the study of the circulation of the world ocean, *J. Comput. Phys., 4,* 347–376, 1969.

Cox, M. D., A primitive equation, three-dimensional model of the ocean, *Tech. Rep. 1,* 143 pp., GFDL Ocean Group, Geophys. Fluid Dyn. Lab., Princeton University, 1984.

Duplessy, J. C., N. J. Shackleton, R. G. Fairbanks, L. Labeyrie, D. Oppo, and N. Kallel, Deep-water source variations during the last climate cycle and their impact on the global deep-water circulation, *Paleoceanography, 3,* 343–360, 1988.

England, M. H., On the formation of Antarctic Intermediate and Bottom Water in ocean general circulation models, *J. Phys. Oceanogr., 22,* 918–926, 1992.

England, M. H., Representing the global-scale water masses in ocean general circulation models, *J. Phys. Oceanogr., 23,* 1523–1552, 1993.

England, M. H., J. S. Godfrey, A. C. Hirst, and M. Tomczak, The mechanism for Antarctic Intermediate Water renewal in a World Ocean model, *J. Phys. Oceanogr., 23,* 1553–1560, 1993.

Haney, R. L., Surface thermal boundary condition for ocean circulation models, *J. Phys. Oceanogr., 1,* 241–248, 1971.

Huang, R. X., Real freshwater flux as the upper boundary condition for the salinity balance and thermohaline circulation forced by evaporation and precipitation, *J. Phys. Oceanogr., 23,* 2428–2446, 1993.

Huang, R. X. and R. L. Chou, Parameter sensitivity study of the saline circulation, *Clim. Dyn.,* in press, 1994.

Huang, R. X., J. R. Luyten, and H. M. Stommel, Multiple equilibrium states in combined thermal and saline circulation, *J. Phys. Oceanogr., 22,* 231–246, 1992.

Maier-Reimer, E., and U. Mikolajewicz, Experiments with an OGCM on the cause of the Younger Dryas, *rep. 39,* pp. 1–13, Max-Planck-Inst. für Meteorol., Hamburg, Germany, 1989.

Marotzke, J., Instability and multiple steady states of the thermohaline circulation, in *Oceanic Circulation Models: Combining Data and Dynamics,* edited by D. L. T. Anderson and J. Willebrand, pp. 501–511, Kluwer, Nowell, Mass., 1989.

Moore, A. M., and C. J. C. Reason, The response of the global ocean general circulation model to climatological surface boundary conditions for temperature and salinity, *J. Phys. Oceanogr., 23,* 300–328, 1993.

Reid, J. L., Jr., Intermediate waters of the Pacific Ocean, *Johns Hopkins Oceanogr. Stud., 2,* 95 pp., 1965.

Stommel, H., Thermohaline convection with two stable regions of flow, *Tellus, 13,* 224–230, 1961.

Toggweiler, J. R., and B. Samuels, Is the magnitude of the deep outflow from the Atlantic Ocean actually governed by Southern Hemisphere winds?, in *The Global Carbon Cycle,* edited by M. Heimann, pp. 303–331, NATO ASI Series, Springer-Verlag, New York, 1993.

Weaver, A. J., and E. S. Sarachik, The role of mixed boundary conditions in numerical models of the ocean's climate, *J. Phys. Oceanogr., 21,* 1470–1493, 1991.

Weaver, A. J., E. S. Sarachik, and J. Marotzke, Freshwater flux forcing of decadal and inter-decadal oceanic variability, *Nature, 353,* 836–838, 1991.

Weaver, A. J., J. Marotzke, P. F. Cummins, and E. S. Sarachik, Stability and variability of the thermohaline circulation, *J. Phys. Oceanogr., 23,* 39–60, 1993.

Welander, P., Thermohaline effects in the ocean circulation and related simple models, in *Large-Scale Transport Processes in Oceans and Atmosphere,* edited by J. Willebrand and D. L. T. Anderson, pp. 163–200, D. Reidel, Norwell, Mass., 1986.

Winton, M., and E. S. Sarachik, Thermohaline oscillations induced by strong steady salinity forcing of ocean general circulation models, *J. Phys. Oceanogr., 23,* 1389–1410, 1993.

Wright, D. G., and T. F. Stocker, A zonally averaged ocean model for the thermohaline circulation, I; Model development and flow dynamics, *J. Phys. Oceanogr., 21,* 1713–1724, 1991.

R. X. Huang, Department of Physical Oceanography, Woods Hole Oceanographic Institution, Woods Hole, MA 02543. (e-mail: Internet: huang@phoenix.whoi.edu)

(Received November 30, 1992; revised June 14, 1993; accepted July 30, 1993.)